Influence of Layered Silicates on the Phase-Separated Morphology of PS−PVME Blends

Koray Yurekli,[†] Alamgir Karim,[‡] Eric J. Amis,[‡] and Ramanan Krishnamoorti*[,†]

Department of Chemical Engineering, University of Houston, Houston, Texas 77204-4004, and Polymers Division, National Institute of Standards and Technology, Gaithersburg, Maryland 20899

Received May 17, 2002

ABSTRACT: The influence of the disk diameter of nanometer thick anisotropic layered silicates on the phase-separated morphology of a near-critical polystyrene (PS)−poly(vinyl methyl ether) (PVME) blend was examined using atomic force microscopy. Films with comparable amounts of thermodynamically equivalent nanoparticles varying only in lateral disk diameters were examined using a temperature gradient method and showed dramatic differences in late-stage morphology. The blends with small disk diameter (30 nm and 0.5 μm) nanoparticles exhibit a pinning of domain sizes and demonstrate an increase in the number of domains with a higher fraction of near circular structures. On the other hand, for layered silicates with large disk diameters (10 μm), the nanoparticles do not affect the morphology of the phase-separated structure and only accelerate the phase separation kinetics. The extent of domain pinning increases with increasing silicate content and results in smaller domains at higher concentrations of silicate.

Introduction

The addition of anisotropic layered silicates to a polymer blend can affect the thermodynamic phase behavior of the blend, the kinetics of phase separation, and the morphology formed in the two-phase region.[1−4] A companion paper will examine the effect of added layered silicate (a hydrophobic organically modified montmorillonite) on the thermodynamic phase behavior of a blend of polystyrene (PS) and poly(vinyl methyl ether) (PVME).[5] The phase behavior, determined from small-angle neutron scattering, static light scattering, and a novel two-dimensional combinatorial method, established that the addition of up to 4 vol % of the layered silicate had a negligibly small effect on the overall blend phase boundaries.

This paper examines the changes to the two-phase morphology of a blend of polystyrene (PS) and PVME by the addition of three different organically modified silicates of varying lateral dimensions. The layered silicates Laponite, montmorillonite, and fluorohectorite, primarily vary in lateral dimensions and possess equivalent disk diameters of 300 Å, 0.5−1.0 μm, and 10 μm, respectively.[6,7] In all three cases, the layer thicknesses (h_0) are identical and equal to 0.95 nm. Laponite and fluorohectorite are synthetically produced while the montmorillonite is a naturally occurring silicate and possesses a larger variation in terms of the lateral size, shape, and isomorphous substitution than the synthetic silicates. Montmorillonite and Laponite have charge exchange capacities (CEC) of 0.9 and 0.75 equiv/kg respectively and were modified with dimethyl dioctadecylammonium. On the other hand, fluorohectorite with a CEC of 1.5 equiv/kg was modified with trimethyl octadecylammonium. The use of a single-stranded surfactant for the high CEC fluorohectorite and a double-stranded surfactant of the same tail length for the low CEC montmorillonite and Laponite is expected to result in similar organic surface coverage and roughly the same liquidlike conformations of the surfactants for the three layered silicates. It is noted that in the thermodynamic theories of Vaia [8,9] and Balazs,[10] the layers are predominantly characterized by their CEC, surface organic coverage, and the conformations of the organic modification before and after mixing with the polymer. Therefore, it is reasonable to expect that the three layered silicates employed in this study are thermodynamically equivalent and that differences in the effectiveness of the three layered silicates to alter the morphology of the phase-separated polymer blend are largely dependent on their lateral dimensions. In fact, this hypothesis is supported by spectroscopic inferences of the surfactant conformations[11] and experimental evidence of mixing reported by Vaia and Giannelis.[8]

Experimental Section

Materials and Sample Preparation. The PS and dPS were obtained from Polymer Source[12] with weight-average molecular weights (M_w) of 96 500 and 102 000 respectively and $M_w/M_n < 1.05$.[13] The PVME has a M_w of 119 000 with a M_w/M_n of ≈2.5. As described in the Introduction, the three organically modified layered silicates are a dimethyl dioctadecylammonium substituted Laponite (2C18L), a dimethyl dioctadecylammonium substituted montmorillonite (2C18 M) and a trimethyl octadecylammonium substituted fluorohectorite (C18F). These organically modified layered silicates were prepared by ion exchange in aqueous ethanol solutions and were verified to contain stoichiometric amounts of organic modifiers.

Temperature Gradient Combinatorial Method. The appropriate amounts of PS and PVME were dissolved in toluene to obtain a near-critical composition of $\phi_{PS} = 0.18$ in a solution that contained ∼0.05 g of polymer and 1 mL of solvent. Enough layered silicate was added to this solution to result in a volume fraction of 0.008 in the composite. To achieve stable blend films, 3 × 4 cm Si wafers were treated with hydrofluoric acid to remove the surface oxide layer and render them hydrophobic. This treatment involved submersion of the wafers in HF for 3 min followed by a 5 min dip in a neutralizing solution followed by extensive washing with deionized water. The polymer blend−layered silicate solution was then flow-coated on the HF-etched Si wafer. The flow-coating method has been described in detail elsewhere,[14] and

[†] University of Houston.
[‡] National Institute of Standards and Technology.

10.1021/ma020755l CCC: $25.00
Published on Web 08/21/2003

it involves spreading of a polymer solution on the wafer by the edge of a spatula followed by the evaporation of the solvent that results in a polymer film. The film thickness is dictated by the concentration of the solution as well as the velocity of the spatula, while the uniformity of the thickness depends on the acceleration. For this study, high accelerations were used to achieve uniform films, and the film thicknesses across the Si wafers for all samples were determined by ellipsometry to be within 600 ± 100 nm. A temperature gradient was applied along the length of the wafer for 15 min on an aluminum stage, under vacuum, with a temperature-controlled fluid running through one end and a cartridge heater at the other hand. The temperatures at the ends of the wafer were ≈100 and 155 °C. Since the critical temperature (T_c) for a PS/PVME blend with such component molecular weights is ≈125 °C,[15] the choice of high and low temperatures allowed the cloud point of the PS/PVME blend to fall close to the middle of the wafer. The wafer was quickly quenched to room temperature, at the end of the annealing, to freeze and preserve the phase-separated morphology.

AFM measurements were performed using a Dimensions 2000 AFM.[12] Scans were taken in tapping mode, at 0.2 Hz with the amplitude set point at approximately 80% of the free oscillation amplitude. The integral gain values ranged from 0.75 to 1; the proportional gain ranged from 1.5 to 2.0. Height and phase angle images were simultaneously collected. A similar set of AFM images corresponding to comparable anneal temperatures, and using the same settings, were taken after immersing the wafers in methanol for a minute. Washing with methanol, which dissolves PVME but is a nonsolvent for PS, resulted in the removal of the PVME-rich phase and a clearer picture of the phase-separated morphology. Therefore, the images taken after the methanol wash were used for the image analysis. These pictures were reduced to gray scale, thresholded to result in binary images, and analyzed using a commercially available image analysis package. Transformations to Fourier space, domain size, and domain shape analyses were performed on these reduced images.

Early Stage Kinetics and Concentration Dependence. The dPS/PVME nanocomposites for these experiments were also prepared by solution mixing as described above. The volume fraction of dPS in the blends was 0.28. The layered silicate concentration ranged from 0 to 4 vol %. The films were cast using a spin coater at 1500 rpm from a 5 mass % solution of the nanocomposite and resulted in ∼700 nm thick films. The annealing was carried out in a vacuum oven to avoid dewetting and degradation. The samples for the concentration dependence experiments were annealed simultaneously in the same vacuum oven to ensure identical exposure times. AFM measurements for these films were carried out using a Nanoscope IIIa AFM and used in the same operational mode as described above.

Results and Discussion

Films of a phase separating near-critical polymer blend, due to the preferential segregation of one or both of the components to the two interfaces (at the Si wafer and at the air surface), can exhibit surface directed spinodal waves perpendicular to the interfaces.[16−19] However, it has also been shown that below a critical film thickness (between 200[17−20] and 1500 nm[21] depending on the blend), the surface-directed phase separation is suppressed.[17−20] In these thin films, for a symmetrically surface segregating blend (i.e., where the same component preferentially wets both interfaces) such as the PS/PVME system studied here, the phase separation occurs laterally and is accompanied by surface height variations[17−20,22] caused by differences in surface tension of the two components.[18] Furthermore, in films thicker than 100 nm, the development of lateral phase separation was found to have kinetics similar to that of bulk spinodal decomposition of an equivalent PS/PVME blend.[18,20]

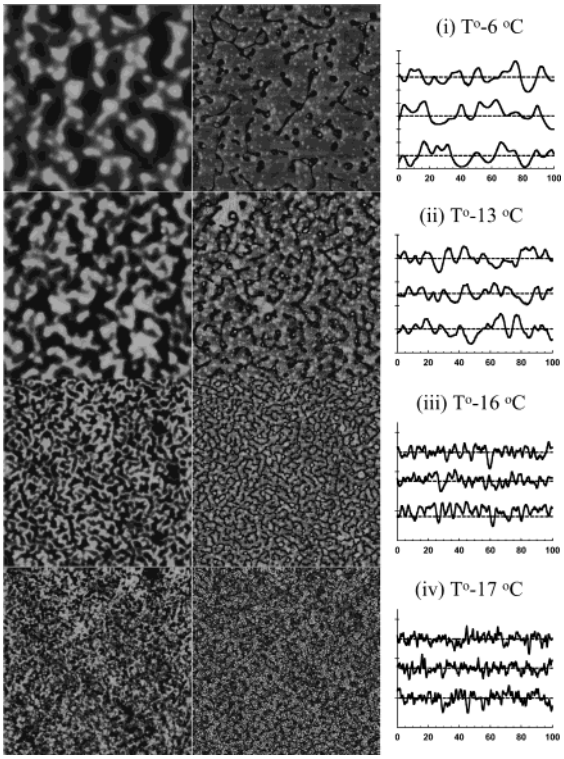

Figure 1. Sequence of 100 μm × 100 μm AFM images showing the evolution of the phase-separated morphology in the $\phi_{PS} = 0.18$ blend film. Three images are shown for each temperature; height image on the left and phase angle in the center and representative line scans of the height image on the right (each tick mark along the ordinate in these line scans correspond to 200 nm). Lighter regions in the height image corresponding to taller features and the darker regions in the phase angle images corresponding to lower phase angles or higher stiffness are thought to be the PS-rich domains. $T_c = T° - 33 \pm 1$ °C, with $T° = 155 \pm 5$ °C.

The evolution of the laterally phase-separated spinodal morphology for the PS/PVME blend (with no added layered silicate) with quench depth is shown in Figure 1, where a sequence of 100 μm × 100 μm atomic force micrographs corresponding to different annealing temperatures is shown. Temperatures on the wafer were determined by measuring distances from the high-temperature wafer edge (with temperature $T°$) and assuming a linear temperature profile. Absolute endpoint temperatures on the film are known to within ± 3 °C and relative temperatures between different locations of the film are known to better than ± 0.1 °C.

At higher temperatures (i.e., deeper into the two-phase region), the spinodal structure coarsens, eventually resulting in PS-rich droplets in a PVME-rich matrix. Height (topography) and phase angle images of the same scanned area are shown on the left and right, respectively. Representative sections from the height image are also shown in Figure 1 to demonstrate the spinodal nature of phase separation.

Temperature sequence of AFM scans of the PS/PVME blends filled with 0.8 vol % 2C18L, 2C18M, and C18F are shown in Figure 2, parts a−c, respectively. While they show the same general features of phase separation, the morphology is not as clearly defined as in the unfilled blend (Figure 1). The presence of the layered silicate possibly leads to large topographical or height fluctuations that obscure the two-phase structures and is consistent with the observations of Giannelis and coworkers on blends of PS and PMMA with layered

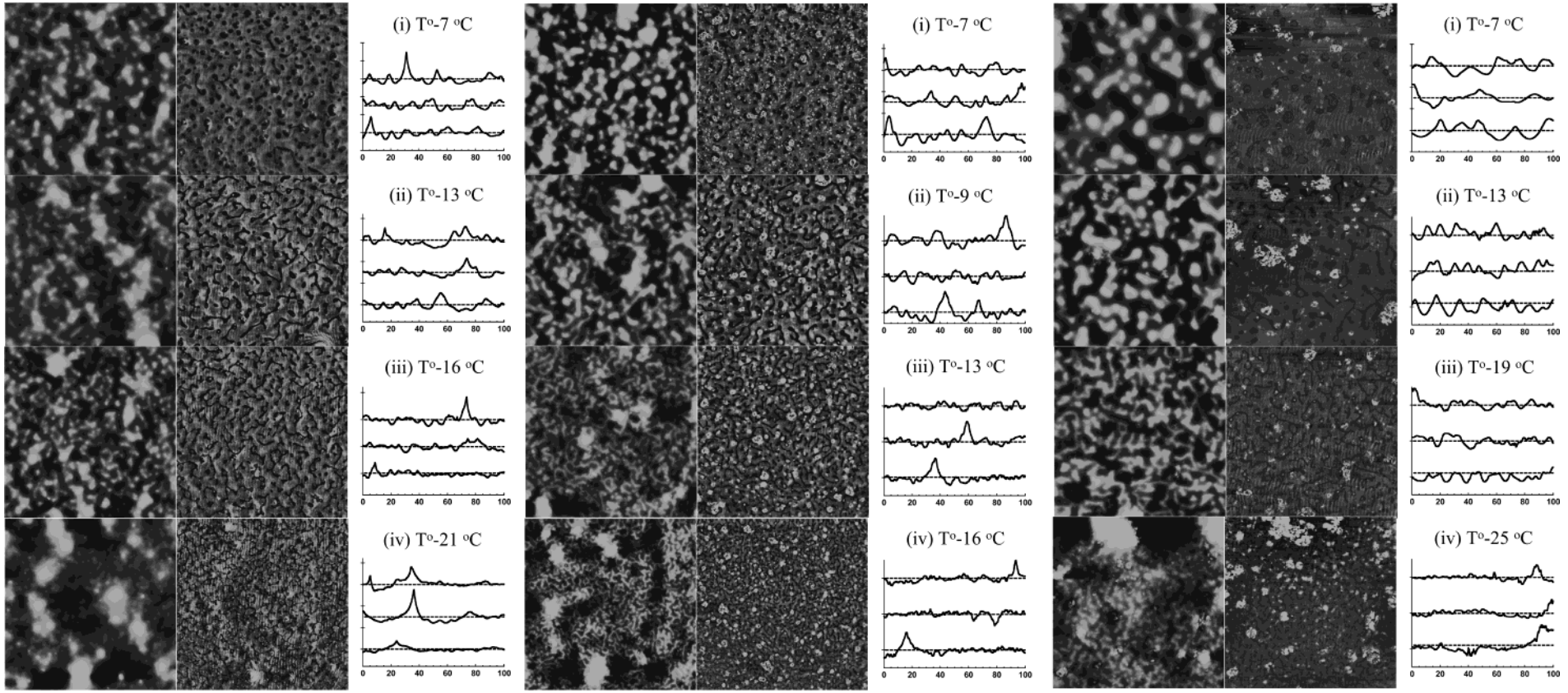

Figure 2. Sequence of 100 μm $\times$ 100 μm height and phase angle AFM images showing the evolution of the phase-separated morphology in the $\phi_{PS} = 0.18$ blend film containing 0.8 vol % 2C18L ($T_c = T° - 33 \pm 1$ °C, with $T° = 155 \pm 5$ °C) (a), 0.8 vol % 2C18M ($T_c = T° - 30 \pm 1$ °C, with $T° = 155 \pm 5$ °C) (b), and 0.8 vol % C18F ($T_c = T° - 34 \pm 1$ °C, with $T° = 155 \pm 5$ °C) (c). Each tick mark along the ordinate in the line scans of this figure and of all the line scans in the following figures corresponds to 500 nm. The height images contain some large features that partially obscure the phase-separated morphology and make image analysis difficult. Also, due to their relatively large size, the C18F tactoids are visible in these images.

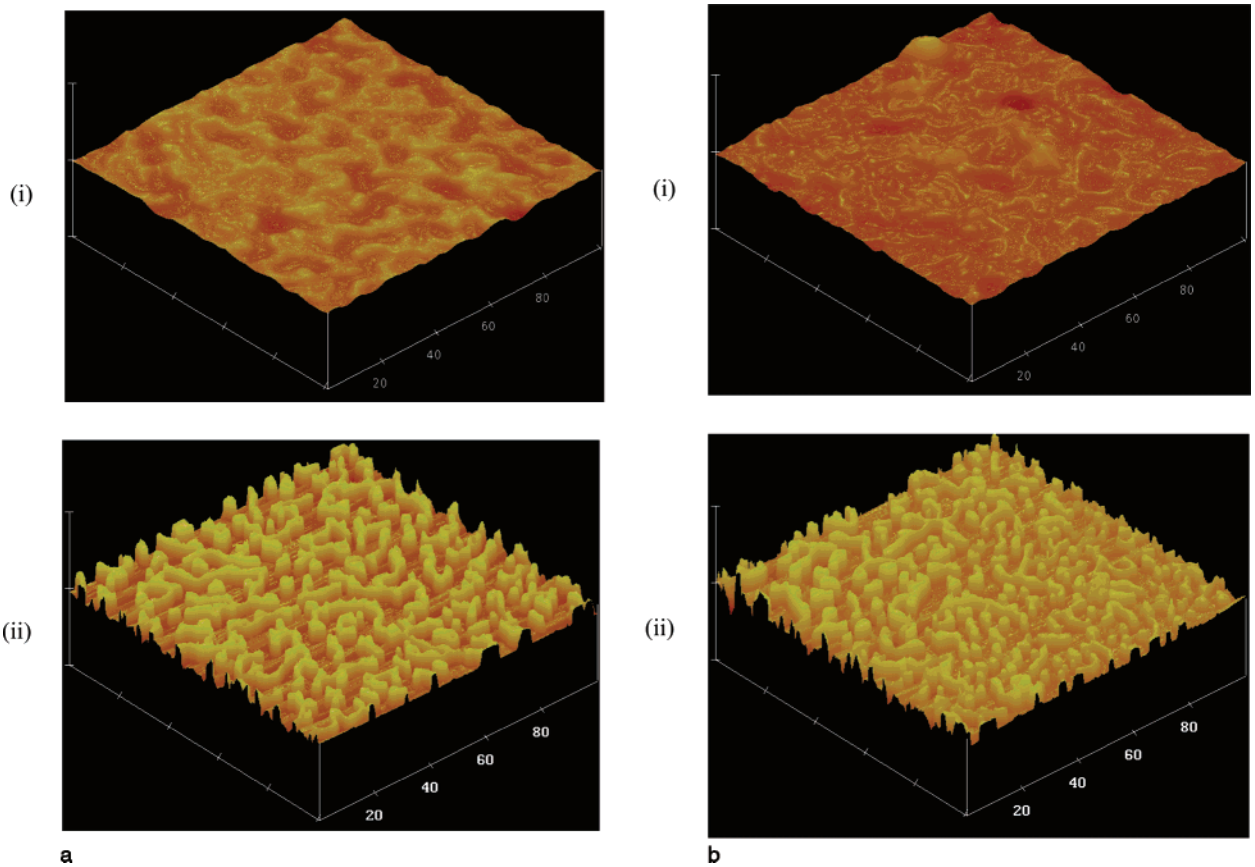

Figure 3. 3D topographical AFM images showing the phase-separated morphology in the $\phi_{PS} = 0.18$ blend film at $T° - 13$ °C (a) and the $\phi_{PS} = 0.18$ blend film with 0.8 vol % 2C18M at $T° - 9$ °C (b). Part i corresponds to annealed films, while part ii refers to images taken after the methanol wash. The height scale in all images is 3 μm, and the lateral dimensions are 100 μm × 100 μm. Note that the phase-separated morphology is clearly visible for the unfilled blend in both cases, although the methanol wash significantly increases the contrast. For the 2C18M-containing blend, on the other hand, the phase-separated morphology is not very well-defined before the methanol wash. This lack of definition compared to the unfilled blend is representative of all images of layered-silicate-containing images.

silicates.[2] The addition of the layered silicates also appears to stabilize the thin polymer films on the Si surface and these film stability issues are discussed separately in the Appendix.

To study the phase separation quantitatively with digital image analysis, it was necessary to obtain more clearly resolved features. This was achieved by immersion of the films in methanol to dissolve and remove the PVME-rich phase, as described in the Experimental Section and demonstrated previously by Ermi et al.[18] and by Stamm et al.[17] The three-dimensional images for the unfilled and 2C18M-containing blends, before and after the methanol wash, are shown in Figure 3 and reveal the improvement in the definition of the PS-rich domains. The removal of the PVME results in a height contrast on the order of 1 μm between the PS and the adjacent bare Si substrate, leading to a sharply defined structure for both the unfilled and particularly for the 2C18M-containing blends. This improvement of definition is representative of the blends containing 2C18L, 2C18M, and C18F, and is attributed to the removal of much of the layered silicate along with the PVME.

The methanol washed AFM scans, complementing the study in Figures 1 and 2, are shown in Figures 4 and 5, respectively. The methanol washed AFM topography scans are used to quantify the influence of the layered silicates on the phase morphology described in the rest of the paper. We caution here that the swelling of the PS-rich domains by the methanol could occur and result in some subtle changes in the shape and size of the domains. However, by maintaining a short and, more importantly, uniform exposure period to methanol, we anticipate that the differences observed between samples are illustrative of the structure prior to the methanol wash.[17,18] The relatively small influence of the methanol washing on the observed morphology is demonstrated in Figure 6 for the unfilled PS/PVME. For deep excursions into the two-phase region, i.e., where phase sizes are large, the power FFT spectra are nearly identical. On the other hand, for temperatures closer to the cloud-point where co-continuous domains are observed, the FFT power spectra for the washed and unwashed sample ($\phi_{dPS} = 0.18$ at $T° - 9$ °C) demonstrate changes in the intensity with peaks at identical values of q^*. This indicates that the methanol wash even for the nanocomposites results in the domain size determination to be unaffected and that the height (or topological) differences between adjacent domains is sharpened.[17,18]

Before comparing the quantitative data for these AFM data that reveal the morphology as a function of quench depth, we ascertain that the blends with the nanoparticles, in fact, undergo spinodal decomposition. The kinetics are studied by examining a set of AFM images of a near-critical dPS−PVME blend corresponding to the early stages of phase separation at constant temperature ($T = 170$ °C) but allowed to anneal for different times. First, at all times studied, the FFT of the AFM data revealed the presence of a dominant wavelength that increased with increasing time. Further, as shown

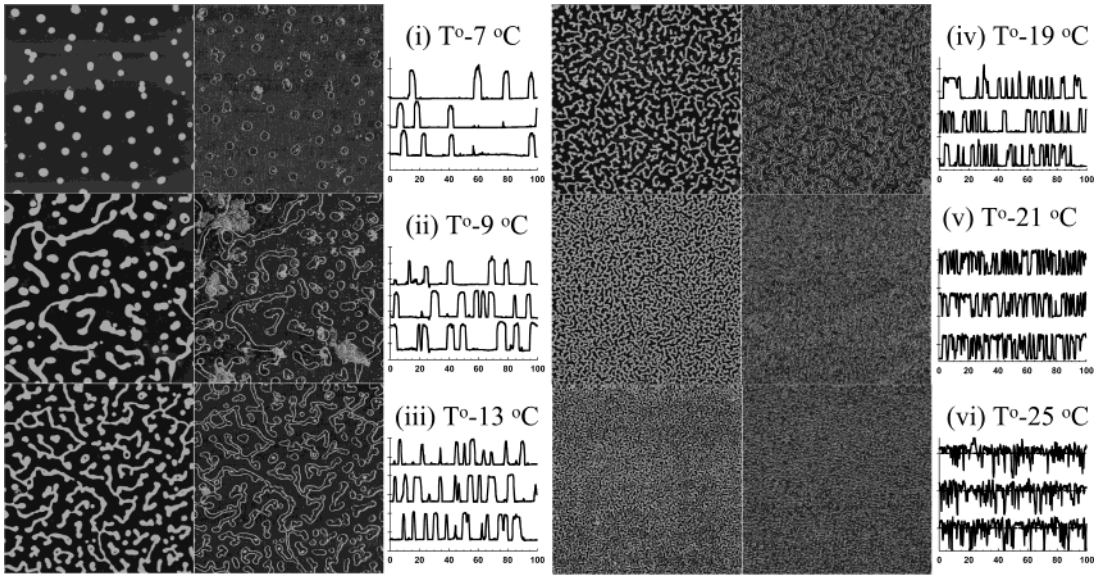

Figure 4. Sequence of 100 μm × 100 μm height and phase angle AFM images showing the evolution of the phase-separated morphology in the methanol-washed $\phi_{PS} = 0.18$ blend film. Methanol wash results in only the PS-rich structures remaining on the SI wafer. $T_c = T° - 33 \pm 1$ °C, with $T° = 155 \pm 5$ °C.

in Figure 7, the characteristic length scale (or dominant wavelength) obtained from the FFT of the AFM images has nearly a $t^{1/3}$ dependence up to 2 min at an annealing temperature of 170 °C.[22] Beyond this, the time dependence becomes stronger, indicative of intermediate stage of spinodal decomposition, and is not fully explored.

We now quantitatively examine the influence of added nanoparticles on the phase-separated morphologies shown in Figures 4 and 5. The basis of comparison between different samples and quench depths, specifically the determination of a parameter to characterize the "extent of phase separation", needs to be clarified. Progression of phase separation is a combination of the quench depth (i.e., the difference between the annealing temperature and the cloud-point temperature), and the annealing time. It has been shown by Takenaka and Hashimoto[23] that parameters that characterize the domain growth such as the maximum intensity (I_{max}) and the location (q^*) of the main peak in a FFT spectrum of spinodal decomposition pattern obey the time−temperature superposition. Exploiting the self-similar nature of the time and temperature dependence of the FFT peak, they created master curves of I_{max} and q^* from data collected at different annealing temperatures as a function of time by using vertical and horizontal shifts.

We use the value of characteristic length of phase separation, q^*, as a measure of the "extent of phase separation". The error in quench depth ($T - T_c$) was $\approx \pm 0.5$ °C and primarily attributed to the breadth of the phase boundary, since temperature differences as small as 0.1 °C can be accurately determined along the wafer. Further, the annealing time was only accurate to ±15 s. It is expected that near T_c, even a small difference in annealing time would result in a large difference in the observed two-phase structure. Therefore, we prefer to use q^* as a measure of the extent of phase separation.

Figure 8 shows the dependence of $1/q^*$ on $1/T - 1/T_{cp}$, where T_{cp} is the cloud point temperature. Although the range of q^* and the number of data points are limited, $1/q^*$ follows a roughly exponential trend for all the blends, with the dependence being considerably weaker for the 2C18L- and 2C18M-filled blends. Notably, for the same range of quench depths and for roughly the same annealing time, the 2C18M- and 2C18L-filled blends exhibit a considerably smaller range of q^* values, suggesting the possibility that the domain growth might be arrested or pinned in those cases.

The length scale of the structure suggests that all samples shown in Figure 8 are in the later stages of spinodal decomposition. Systematic changes in the quench depth systematically change the thermodynamic driving force for phase separation. This driving force for phase separation is given as $(\chi(T) - \chi_s(T_c))$, and because $\chi \propto -1/T$, the driving force for phase separation can reasonably be represented as $(1/T_{cp} - 1/T)$. Thus, it is hardly surprising that we observe that at constant annealing times, the domain size has a roughly exponential dependence on $(1/T_{cp} - 1/T)$. Such an Arrhenius-type behavior has been previously documented for the kinetics of spinodal phase separation in LCST systems.[24]

This idea of domain pinning by the addition of nanoparticles is further explored by examining the effect of layered-silicate concentration on q^* for a dPS/PVME blend annealed at a fixed temperature of 177 °C for 15 min, corresponding to intermediate or late stage phase separation (all of the measurements were performed simultaneously, thereby eliminating any differences in time and temperature of annealing). The AFM images for the blends with different concentrations of 2C18L are shown in Figure 9. The concentration dependence of q^* for these blends and those for similar blends with 2C18M (held at identical temperature and time) are shown in Figure 10. Two features are striking: (a) The characteristic length scale of phase separation decreases with increasing nanoparticle concentration and (b) the larger nanoparticle (2C18M) results in larger domain sizes. In the companion paper we have demonstrated that the thermodynamic phase boundaries are essentially unaffected by the addition of up to 4% nanoparticle and suggests that morphological consequences observed are a result of a change in kinetics or a pinning phenomenon rather than caused by changes in thermodynamics.

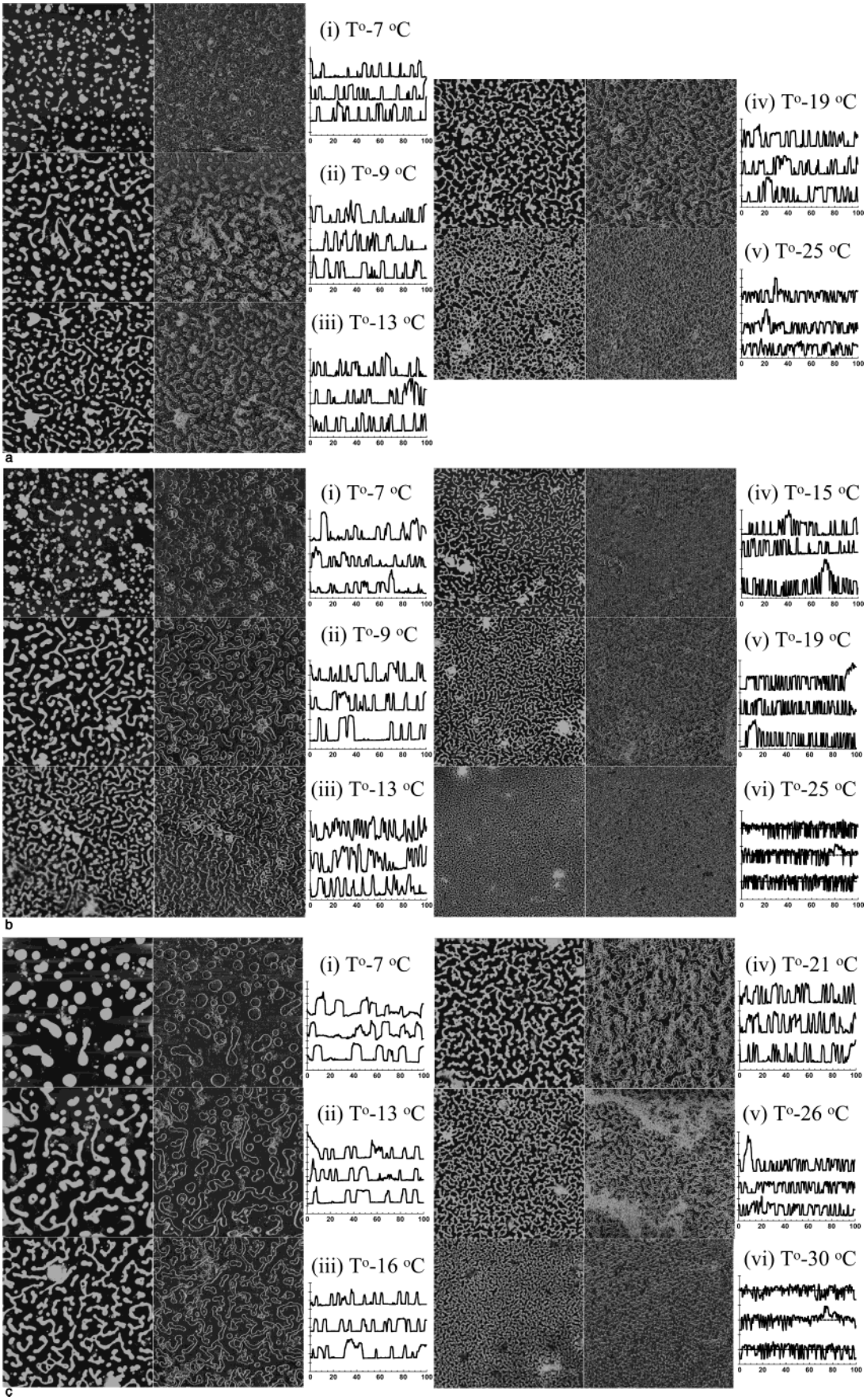

Figure 5. Sequence of 100 μm $\times$ 100 μm height and phase angle AFM images showing the evolution of the phase-separated morphology in the methanol washed $\phi_{PS} = 0.18$ blend film containing 0.8 vol % 2C18L ($T_c = T° - 33 \pm 1$ °C, with $T° = 155 \pm 5$ °C) (a), 0.8 vol % 2C18M ($T_c = T° - 30 \pm 1$ °C, with $T° = 155 \pm 5$ °C) (b), and 0.8 vol % C18F ($T_c = T° - 34 \pm 1$ °C, with $T° = 155 \pm 5$ °C) (c). The methanol wash results in clear definition of the phase-separated morphology. Also, a significant fraction of the C18F tactoids that were observed in Figure 2c is removed.

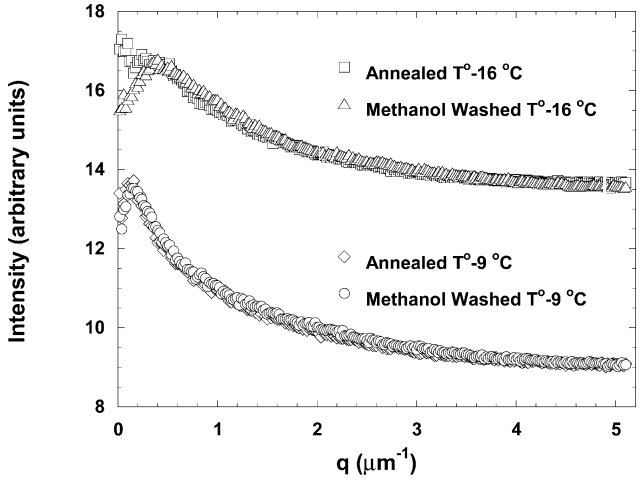

Figure 6. FFT power spectra for annealed and methanol washed $\phi_{PS} = 0.18$ blend films with no layered silicates at two temperatures. Note that while the intensities obtained from the film annealed closer to the cloud-point are lower than those obtained from its methanol washed counterpart, the location of the peak, q^*, is not affected by the removal of the PVME.

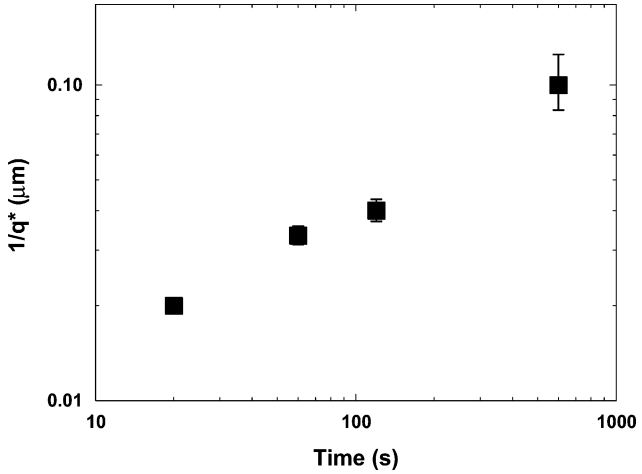

Figure 7. Characteristic length scale ($1/q^*$) of the phase-separated structure in a blend film with $\phi_{dPS} = 0.28$ as a function of time, obtained from FFT of AFM images. The straight line represents a $t^{1/3}$ dependence for $1/q^*$. The kinetics are consistent with early stage spinodal decomposition.

Returning to the quantification of the phase-separated morphologies observed in the temperature gradient experiments; the peak intensity and the breadth in the FFT spectra reveal information about the correlation and regularity of the domain structure. The FFT spectra for the data presented in Figures 4 and 5 were fitted to a combination of Gaussian and Lorentzian functions with a linear background. A peak-fitting software was used to obtain the intensity maximum (I_{max}), and left and right full width at half-maximum (fwhm) values. The left and right wings were fitted independently using variable fractions of a Gaussian and a Lorentzian function. The results of the fits for all the samples are shown in Figure 11. I_{max} scales roughly linearly with $\ln(1/q^*)$ for all blends, which considering Figure 8, translates into a linear dependence on $(1/T - 1/T_{cp})$. Also, in agreement with Takenaka and Hashimoto's[23] results described above, the data for all the blends collapse onto a single curve, and this suggests that the choice of q^* as a measure of the extent of phase separation is valid. The fwhm values, on the other hand, decrease as the phase separation progresses (i.e., $1/q^*$ increases), and the morphologies become sharper. It is noteworthy that the data for the 2C18L-filled blend has a stronger dependence of average fwhm on q^* than the other three blends.

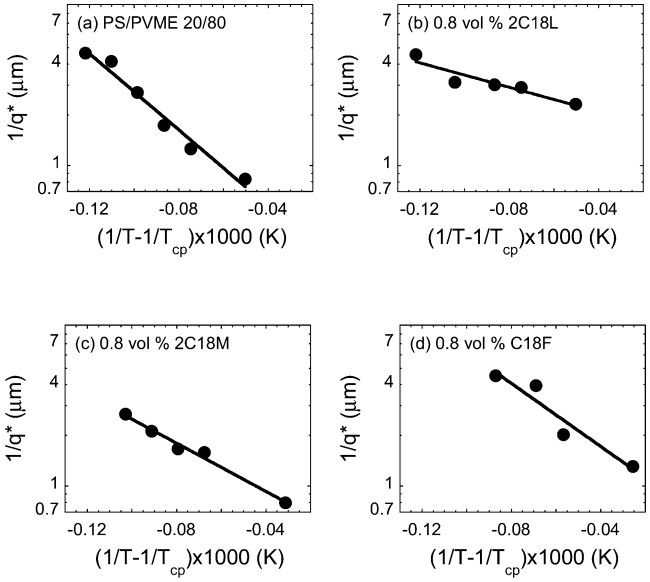

Figure 8. Change in the characteristic length scale of the phase-separated morphology as a function of the distance from the cloud-point temperature shown in a semilog plot for the $\phi_{PS} = 0.18$ film containing: no layered silicate (a), 0.8 vol % 2C18L (b), 0.8 vol % 2C18M (c), and 0.8 vol % C18F (d). The data for all samples are fitted with exponential functions, and the power of the exponent is significantly smaller for the 2C18L- and 2C18M-containing blends. Linear fits to the data reveal a slope of ≈0.35 for the unfilled $\phi_{PS} = 0.18$ and the C18F-containing blend, while the slope for the 2C18L- and 2C18M-containing blends is significantly lower at ≈0.15.

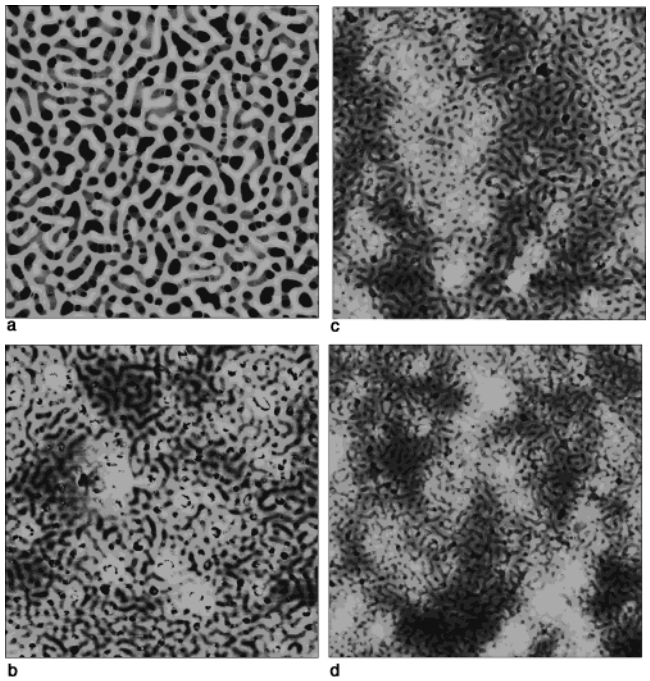

Figure 9. Sequence of 100 μm × 100 μm AFM images showing the phase-separated morphology after 15 min of annealing at 177 °C for the unfilled $\phi_{dPS} = 0.28$ blend (a) and the nanocomposites containing 0.8 (b), 2.0 (c), and 4.0 vol % (d) of 2C18L (30 nm diameter). The phase-separated structure in the nanocomposites is of a smaller length scale than that of the unfilled blend.

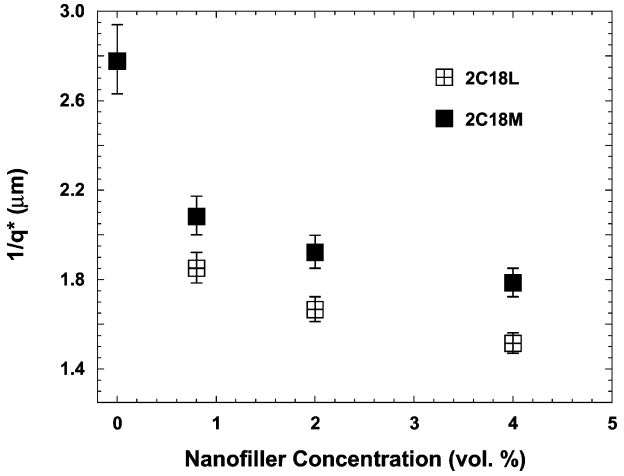

Figure 10. Characteristic length scale ($1/q^*$) of the phase-separated structure in a blend film with $\phi_{dPS} = 0.28$ as a function of 2C18L and 2C18M concentration, obtained from FFT of AFM images. The effect of the layered silicate on the phase-separated morphology increases with the concentration. For a given concentration, the 2C18L has a larger effect than the 2C18M.

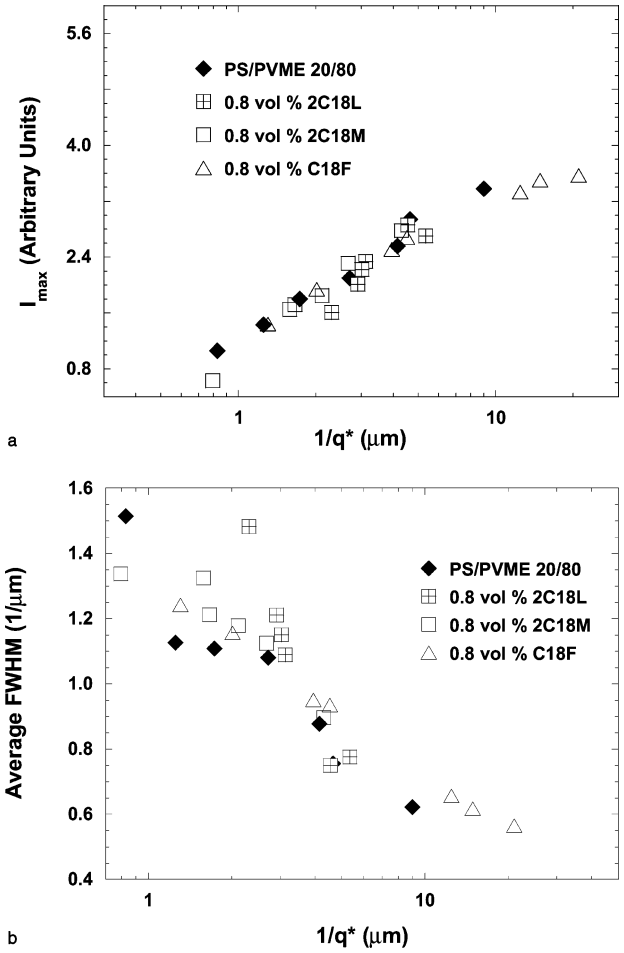

Figure 11. Maximum intensities (a) and the averages of the left and right fwhm (b) of the peak in the Fourier power spectra graphed against $1/q^*$ for the unfilled $\phi_{PS} = 0.18$ blend and the nanocomposites with 0.8 vol % 2C18L, 2C18M, and C18F. A lower $1/q^*$ value corresponds to a smaller length scale and therefore a less developed phase-separated morphology.

The extent of influence exerted by the three layered silicates on the morphology is quantitatively examined by comparing the size and shape of the phase-separated domains. The shape of the phase-separated domains are characterized based on the form factor, defined as

$$f = \frac{4\pi(\text{area})}{(\text{perimeter})^2} \quad (1)$$

with f having a value of 1 for a circle and a value less than unity for elongated structures or structures containing arms. A comparison of the size distribution of the domains and the distribution of form factors for the phase-separated domains in the four samples at comparable values of q^* ($q^* \approx 0.2\ \mu m^{-1}$ and Figures 4(iii), 5a(ii), 5b(ii), and 5c(iii)) are presented in Figures 12 and 13. These images are representative of the phase-separated morphologies in the intermediate stage. Such an analysis could not be performed on the early stage phase-separated morphologies, since they are co-continuous and do not result in individual distinct domains.

The 2C18L- and 2C18M-containing blends show size distributions of the domains and distribution of form factors that are significantly different from that of the unfilled blend. These blends have a larger number of domains per unit area (almost twice as many as the unfilled blend) and a greater propensity for these domains to be small. Additionally, these blends contain a significantly larger fraction of domains with form factors close to unity (i.e., 0.9 and greater). On the other hand, the number of domains, size and form factor distributions for the C18F containing blend are similar to those for the unfilled blend.

It is clear that the addition of layered silicates has a significant impact on the phase-separated morphologies of a near-critical PS−PVME blend. Moreover, the disk diameter of the layered silicates (otherwise thermodynamically equivalent) appears to have a significant influence on the changes observed, with nearly no influence observed for the 10 μm diameter layers and the largest influence for the 30 nm diameter layers. Finally, for 2C18L and 2C18M, the extent of phase separation is inversely proportional to the silicate concentration.

Balazs and co-workers have studied the phase separation of a binary polymer blend in the presence of hard, mobile and hard, immobile particles using a kinetic theory and computer simulations.[3,4,25,26] In addition to the disruption of the bicontinuous spinodal structure,[25,27] nanoparticles also lead to a slowing down of the domain growth in the late stages of spinodal decomposition.[3,4,25] It should be noted that in those simulations the slowing down of the domain growth occurred only when there was preferential wetting of the nanoparticles by one of the blend components. While, as discussed previously, both polymers have slightly attractive interactions with the layered silicates and addition of up to 4 vol % layered silicate left the phase diagram unaffected, the PVME is expected to have marginally better interactions with the layered silicates. In fact, this is qualitatively observed from higher magnification AFM images, such as the one shown in Figure 14, where the layered silicates are shown to reside preferentially in the PVME-rich phase or more accurately in the holes created by the methanol washing of the PVME. Thus, on the basis of the simulations and the AFM data for the nanoparticle filled PS/PVME blends, it might be expected that the nanoparticles would cause a slowing down of domain growth and disruption of the bicontinuous spinodal structure as observed.

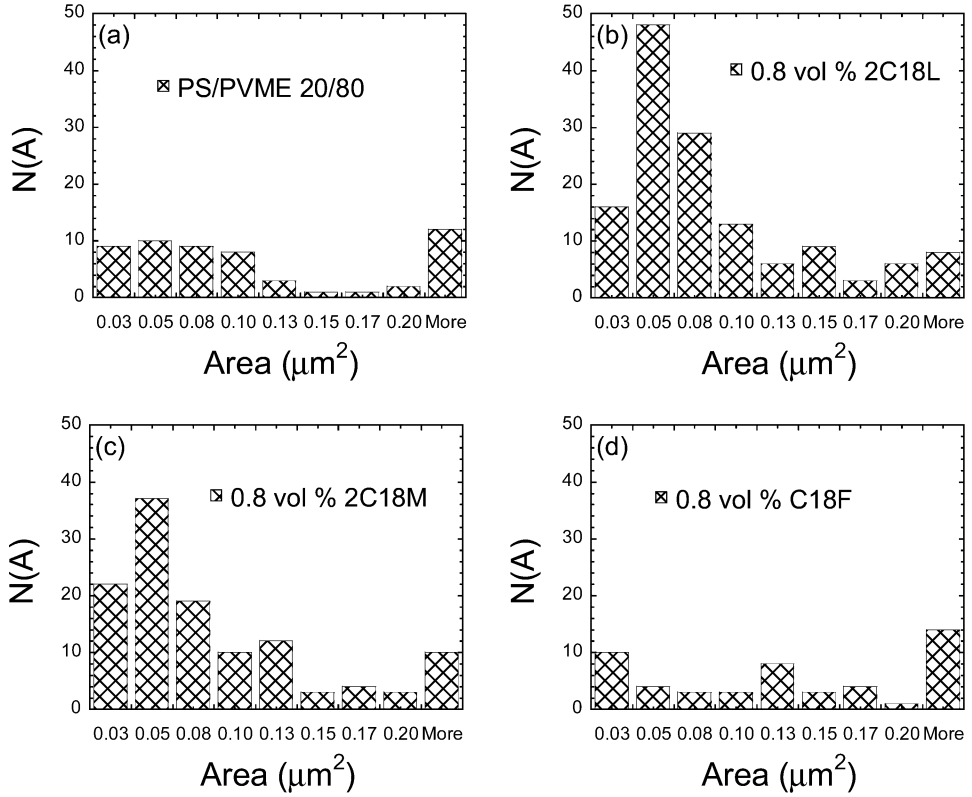

Figure 12. Number distribution of domain sizes ($N(A)$) for the unfilled $\phi_{PS} = 0.18$ blend (a) and the nanocomposites containing 0.8 vol % 2C18L (b), 2C18M (c), and C18F (d). The 2C18L- and 2C18M-containing films have significantly different distributions from the unfilled blend film and the C18F nanocomposite with more domains of smaller sizes.

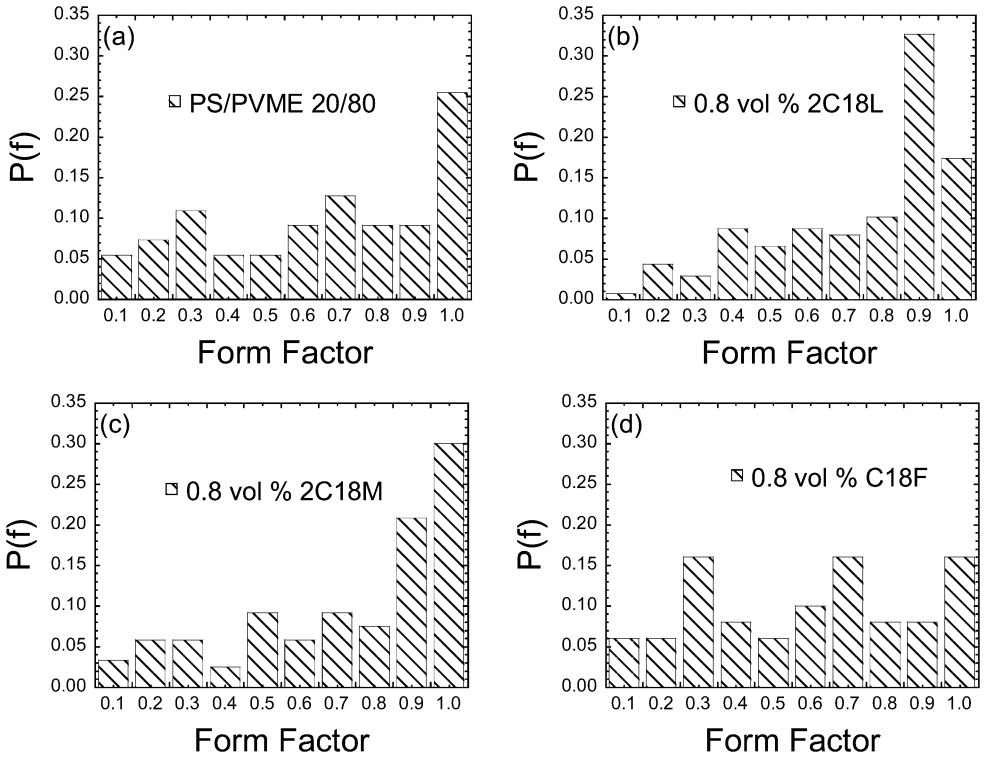

Figure 13. Probability distribution of form factors ($P(f)$) for the unfilled $\phi_{PS} = 0.18$ blend (a) and the nanocomposites containing 0.8 vol % 2C18L (b), 2C18M (c), and C18F (d). The 2C18L- and 2C18M-containing films have significantly different distributions from the unfilled blend film and the C18F nanocomposite with more features of form factors close to unity.

Moreover, according to Balazs et al. the slowing down of the domain growth by pinning occurs when the characteristic domain size becomes comparable to the interparticle distance.[4] In the case of mobile particles, the particles are concentrated in the preferentially wet component and act as obstacles to the motion of interfaces and inhibit the growth of the domains of the other component.[4] For immobile particles, the growths of domains of both components are affected.[3,26] It is thought that this pinning mechanism is the reason for

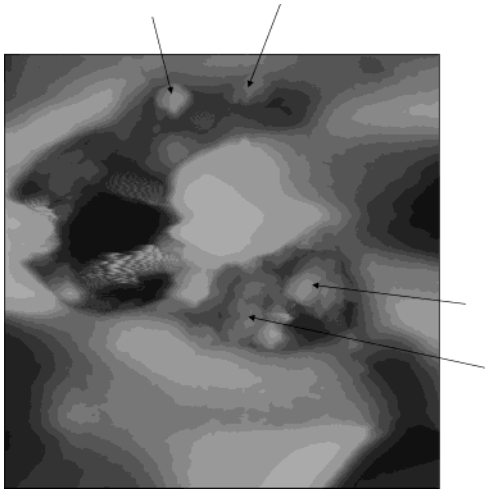

Figure 14. 5.7 μm × 5.7 μm AFM image showing the phase-separated morphology after 15 min of annealing at 177 °C for the nanocomposite with $\phi_{DPS} = 0.28$ and containing 2.0 vol % 2C18L. Note that the layered-silicate particles (marked by arrows) seem to favor the PVME-rich phase.

the observed slower coarsening of the domain structure for the blends with 2C18L and 2C18M. The domains in the C18F containing film, on the other hand, grow at the same rate as those of the unfilled blend. This is most likely because of the fewer particles in the C18F-filled blend (because of poorer breakdown on the tactoids) resulting in a large interparticle distance and the particles being relatively immobile. In this context, we note the results of earlier work on the phase behavior of polymers with these three organically modified layered silicates have revealed a propensity for the C18F to remain intercalated while the 2C18L is completely exfoliated and the 2C18M lies between in terms of structural order.[7] Further, at identical loadings of the silicate, the overlap concentration for exfoliated 2C18L layers is about 5 vol %, which is roughly 2 orders of magnitude larger than that for C18F.[28] Finally, the C18F should also be considered to be a immobile object because of the large particle diameter.[29]

The importance of a large number of dispersed nanoparticles is further illustrated by the concentration dependence experiments as summarized in Figure 10. Up to a loading of 4.0 vol %, both 2C18L- and 2C18M-containing nanocomposites show a less developed phase-separated structure with increasing layered-silicate concentration. In the absence of any perturbation to the thermodynamic behavior of the blends, we suggest that this is because of the larger number of pinning points present in the nanocomposites with higher concentrations of filler. For the same reason, the 2C18L, which has a better dispersion and hence more dispersed nanoparticles, is more effective at stunting morphology growth.

Concluding Remarks

AFM topography images of PS/PVME blends annealed at different temperatures are analyzed quantitatively to determine the effects of three different organically layered silicates differing only in their lateral dimension on the kinetics of phase-separation and phase-separated morphologies. The phase separation of these near-critical blends proceeds by spinodal decomposition even with added nanoparticles. The annealing temperature dependence of $1/q^*$, the characteristic length scale of spinodal decomposition reveals that the presence of 2C18L (30 nm) and 2C18M (0.5−1.0 μm) slows phase-separation kinetics while the C18F (5 μm) has no noticeable effect. The slowing down of the kinetics by the layered silicates is attributed to a pinning mechanism demonstrated by Balazs and coworkers' computer simulations.[3,4,27] Size and shape analysis of the micrographs shows that the same trend applies to the phase-separated morphology. 2C18L and 2C18M containing blends have markedly different morphologies from the unfilled and the C18F-containing films with more small and circular domains. The dependence of these influences on the lateral size of the silicate layers is explained by more exfoliation and better dispersion for silicates with smaller lateral dimensions. Experiments carried out as a function of the layered-silicate concentration at a fixed annealing temperature also support this hypothesis. It is found that the pinning of the phase-separated structure becomes more pronounced as the layered-silicate diameter goes down and the concentration goes up. Certainly these effects must also depend on the relative wetting of the surfaces by the polymers and in the case examined, the silicates are probably only marginally more compatible with the PVME than PS. These effects would be significantly enhanced and become more pronounced for cases where there is a large preferential attraction of one of the polymer components to the silicate surface.

Acknowledgment. The authors would like to thank Dr. Barry Bauer for generously donating the PVME and Dr. Amit Sehgal, Prof. Carson Meredith, and Dr. Archie P. Smith for their help with the combinatorial experiments. K.Y. and R.K. would also like to thank the National Science Foundation (DMR-9875321) and NIST for funding this research.

Appendix

As mentioned in the preceding paper, the presence of 0.8 vol % 2C18M was shown to have a stabilizing effect on the dewetting of the dPS/PVME blend on a Si wafer. The results of two additional experiments are presented here to support that observation. The first experiments were performed with two low molecular weight PS (M_w = 3700) films on hydrophobic (HF etched) Si wafers; one with no added layered silicate and the other with 0.8 vol % 2C18M. The films were flow coated with a small thickness gradient from 50 ± 5 to 100 ± 5 nm in thickness. A temperature gradient was applied under vacuum along the other axis for 150 min under vacuum. Optical images obtained using a 2.5× objective lens for these films are shown in Figure 14, parts a and b, respectively. Although complete dewetting is not observed in either case due to the hydrophobic treatment of the Si wafer, the film is clearly more disrupted in the case of the unfilled PS.

The second experiment examined the influence of nanoparticles on the dewetting of a blend of PS and PVME with a $\phi_{PS} = 0.18$. Two ≈30 nm thick films of the blend, one of them containing 0.8 vol % 2C18M, were cast on Si wafers, which had the SiO_2 layer intact. A temperature gradient from 105 to 180 °C was applied under vacuum for approximately 30 min to both films. Figures 16 and 17 show optical microscopy images of both films at two locations using a 20× objective lens. For the unfilled polymer blend film, it is observed that phase separation and dewetting are linked. That is, the

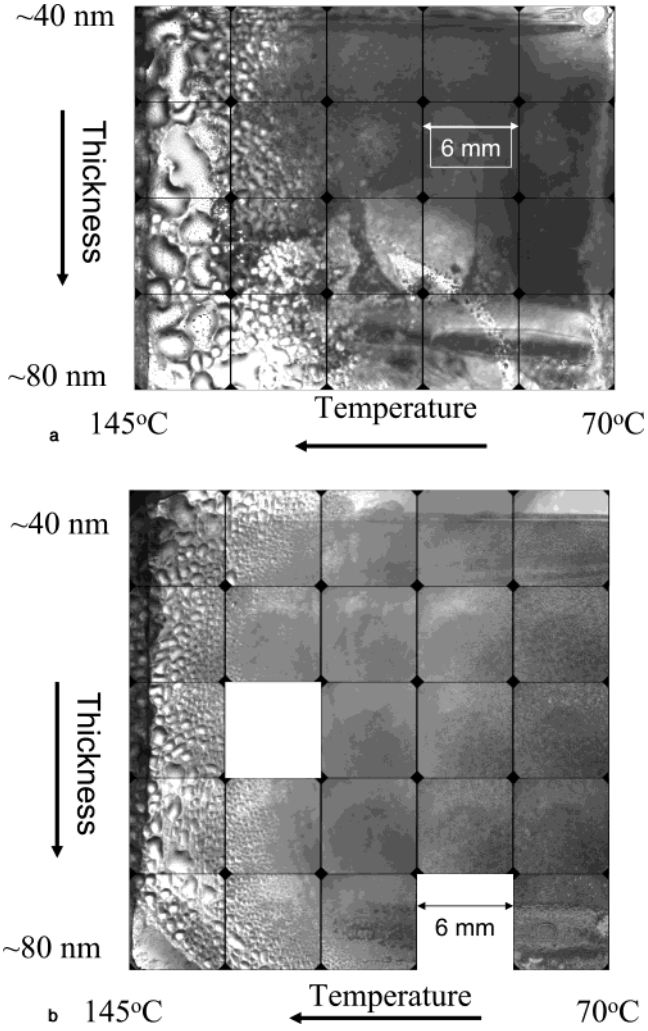

Figure 15. 2.5× magnified optical microscopy images of the low molecular weight PS ($M_w = 3680$) with no layered silicate (a) and 0.8 vol % 2C18M (b) on hydrophobic Si wafers. As expected, film disruption occurs most strongly at higher temperatures and larger thicknesses. Also, the presence of the layered silicate suppresses the dewetting significantly.

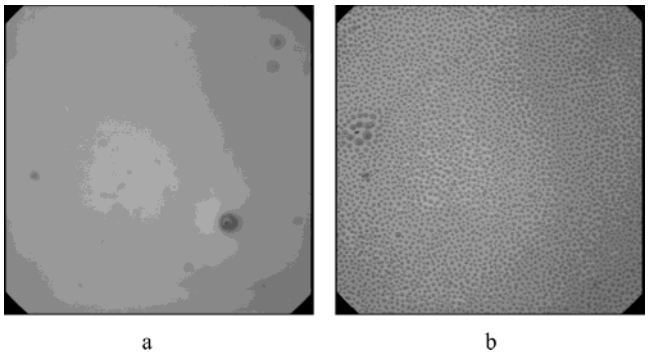

Figure 16. 20× magnified optical microscopy images (750 × 750 μm) from the one-phase (a) and two-phase (b) regions of the unfilled $\phi_{PS} = 0.18$ film cast on a cleaned Si wafer retaining the oxide layer. After 30 min of heating, the two-phase region shows extensive dewetting while the single-phase region is stable.

one-phase region shown in Figure 16a shows a stable film, while above the cloud-point temperature at 135 °C (Figure 16b) the circular patterns with refractive rings characteristic of dewetting appear. This interplay between phase separation and film rupture has been well-documented.[17,30] Figure 17a shows that in the case

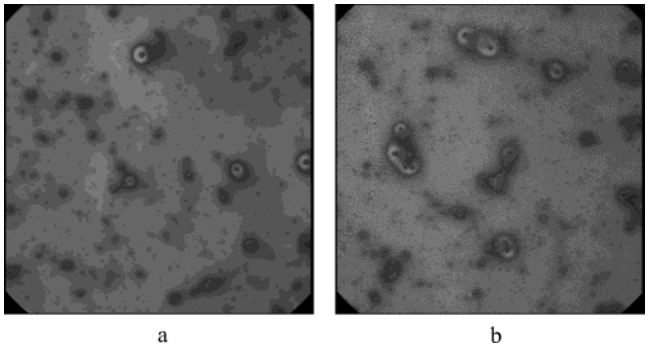

Figure 17. 20× magnified optical microscopy images (750 × 750 μm) from the one-phase (a) and two-phase (b) region of the $\phi_{PS} = 0.18$ film with 0.8 vol % 2C18M cast on a cleaned Si wafer retaining the oxide layer. After 30 min of heating the film is stable in both single-phase and two-phase regions.

of the 2C18M-containing sample, the single-phase film is not as smooth as the unfilled polymer blend. This is not surprising since the lateral dimensions of 2C18M are much larger than the film thickness, so any tactoids that are not completely parallel to the surface will result in surface roughness. Above the cloud-point temperature, however, 2C18M stabilizes the wetting behavior of the film with respect to that observed for the unfilled blend. Compared with Figure 16b, the structures in Figure 17b are smaller and resemble a phase-separated morphology more than dewet holes or islands.

Previous studies have shown that the influence of fillers on the stability of polymeric thin films depends on several experimental parameters.[31−34] In particular, Sharma et al.[33] and Barnes et al.[34] have demonstrated that the addition of nanoparticles can lead to the stabilization of a polymer thin film. Sharma et al.[33] have found that the effect of the filler on dewetting is related to the filler−polymer interactions, with strong favorable interactions leading to an arrest of dewetting. The mechanism of stabilization is thought to be through interfacial pinning since the particles are observed to segregate to the edges of the holes. For the samples reported in this Appendix, the polymers and the added nanoparticles possess attractive interactions and there are no available highly mobile excess alkylammonium surfactants that have been previously implicated in decreasing thin film stability.[32] Thus, it would be anticipated that the stabilization of dewetting for the samples reported here is likely to be due to interfacial pinning and possibly a slowing down because of kinetic parameters such as a local increase in the viscosity.

References and Notes

(1) Lee, B. P.; Douglas, J. F.; Glotzer, S. C. *Phys. Rev. E* **1999**, *60*, 5812−5822.
(2) Ji, G.; Clement, F.; Giannelis, E. P. *Mater. Res. Soc. Symp. Proc.* **2001**, *661*, KK10.11.11−KK10.11.19.
(3) Ginzburg, V. V.; Peng, G.; Qiu, F.; Jasnow, D.; Balazs, A. C. *Phys. Rev. E* **1999**, *60*, 4352−4359.
(4) Ginzburg, V. V.; Qiu, F.; Paniconi, M.; Peng, G.; Jasnow, D.; Balazs, A. C. *Phys. Rev. Lett.* **1999**, *82*, 4026−4029.
(5) Yurekli, K.; Karim, A.; Amis, E. J.; Krishnamoorti, R. *Macromolecules* **2003**, in press.
(6) Silva, A. S.; Mitchell, C. A.; Tse, M. F.; Wang, H.-C.; Krishnamoorti, R. *J. Chem. Phys.* **2001**, *115*, 7166−7174.
(7) Krishnamoorti, R.; Silva, A. S.; Mitchell, C. A. *J. Chem. Phys.* **2001**, *115*, 7175−7181.
(8) Vaia, R. A.; Giannelis, E. P. *Macromolecules* **1997**, *30*, 8000−8008.
(9) Vaia, R. A.; Giannelis, E. P. *Macromolecules* **1997**, *30*, 7990−7999.

(10) Balazs, A. C.; Singh, C.; Zhulina, E. *Macromolecules* **1998**, *31*, 8370−8381. Lyatskaya, Y.; Balazs, A. C. *Macromolecules* **1998**, *31*, 6676−6680. Balazs, A. C.; Singh, C.; Zhulina, E.; Lyatskaya, Y. *Acc. Chem. Res.* **1999**, *32*, 651−657.
(11) Vaia, R. A.; Teukolsky, R. K.; Giannelis, E. P. *Chem. Mater.* **1994**, *6*, 1017−1022.
(12) Certain equipment and instruments or materials are identified in the paper in order to adequeately specify the experimental details. Such identification does not imply recommendation by the National Institute of Standards and Technology, nor does it imply that the materials are necessarily the best available for the purpose.
(13) According to ISO 31-8, the term molecular weight has been replaced by "relative molecular mass" M_r. Thus, if this nomenclature and notation were to be followed in this publication, one would write $M_{r,w}$ instead of the historically conventional M_w for the weight-average molecular weight, with similar changes for M_n, and it would be called the "weight average relative molecular mass." The older, more conventional notation, rather than the ISO notation, has been employed for this publication.
(14) Meredith, C. J.; Smith, A. P.; Karim, A.; Amis, E. J. *Macromolecules* **2000**, *33*, 9747−9756.
(15) Ubrich, J. M.; Ben Cheikh Larbi, F.; Halary, J. L.; Monnerie, L.; Bauer, B. J.; Han, C. C. *Macromolecules* **1986**, *19*, 810−815. Wagler, T.; Rinaldi, P. L.; Han, C. D.; Chun, H. *Macromolecules* **2000**, *33*, 1778−1789.
(16) Krausch, G.; Dai, C.-A.; Kramer, E. J.; Marko, J. F.; Bates, F. S. *Macromolecules* **1993**, *26*, 5566−5571.
(17) Muller-Buschbaum, P.; Gutmann, J. S.; Stamm, M. *Macromolecules* **2000**, *33*, 4886−4895.
(18) Ermi, B. D.; Karim, A.; Douglas, J. F. *J. Polym. Sci., Part B: Polym. Phys.* **1998**, *36*, 191−200.
(19) Karim, A.; Slawecki, T. M.; Kumar, S. K.; Douglas, J. F.; Satija, S. K.; Han, C. C.; Russel, T. P.; Liu, Y.; Overney, R.; Sokolov, J.; Rafailovich, M. H. *Macromolecules* **1998**, *31*, 1.
(20) Sung, L.; Karim, A.; Douglas, J. F.; Han, C. C. *Phys. Rev. Lett.* **1996**, *76*, 4368.
(21) Wang, H.; Composto, R. J.; Hobbie, E. K.; Han, C. C. *Langmuir* **2001**, *17*, 2857−2860.
(22) Cabral, J. T.; Higgins, J. S.; Yerina, N. A.; Magonov, S. N. *Macromolecules* **2002**, *35*, 1941−1950. Cabral, J. T.; Higgins, J. S.; McLeish, T. C. B.; Strausser, S.; Magonov, S. N. *Macromolecules* **2001**, *34*, 3748−3756.
(23) Takenaka, M.; Hashimoto, T. *J. Chem. Phys.* **1992**, *96*, 6177−6190.
(24) Viville, P.; Biscarini, F.; Bredas, J. L.; Lazzaroni, R. *J. Phys. Chem. B* **2001**, *105*, 7496−7507.
(25) Balazs, A. C.; Ginzburg, V. V.; Qiu, F.; Peng, G.; Jasnow, D. *J. Phys. Chem. B* **2000**, *104*, 3411−3422.
(26) Qiu, F.; Peng, G.; Ginzburg, V. V.; Balazs, A. C.; Chen, H.-Y.; Jasnow, D. *J. Chem. Phys.* **2001**, *115*, 3779−3784.
(27) Balazs, A. C. *Curr. Opin. Colloid Interface Sci.* **2000**, *4*, 443−448.
(28) Mitchell, C. A.; Krishnamoorti, R. *J. Polym. Sci., Part B: Polym. Phys. Ed.* **2002**, *40*, 1434−1443.
(29) Ren, J.; Casanueva, B. F.; Mitchell, C. A.; Krishnamoorti, R. *Macromolecules* **2003**, *36*, 4188−4194.
(30) Newby, B.-M. Z.; Wakabayashi, K.; Composto, R. J. *Polymer* **2001**, *42*, 9155−9162.
(31) Cole, D. H.; Shull, K. R.; Baldo, P.; Rehn, L. *Macromolecules* **1999**, *32*, 771−779. Limary, R.; Swinnea, S.; Green, P. F. *Macromolecules* **2000**, *33*, 5227−5234. Karapanagiotis, I.; Evans, D. F.; Gerberich, W. W. *Langmuir* **2001**, *17*, 3266−3272. Stange, T. G.; Evans, D. F.; Hendrickson, W. A. *Langmuir* **1997**, *13*, 4459−4465.
(32) Limary, R.; Green, P. F. In *Polymer Nanocomposites: Synthesis, Characterization, and Modeling*; Krishnamoorti, R., Vaia, R. A., Eds.; ACS Symposium Series 804; American Chemical Society: Washington, DC, 2001.
(33) Sharma, S.; Rafailovich, M. H.; Peiffer, D.; Sokolov, J. *Nano Lett.* **2001**, *10*, 511−514.
(34) Barnes, K. A.; Karim, A.; Douglas, J. F.; Nakatani, A. I.; Gruell, H.; Amis, E. J. *Macromolecules* **2000**, *33*, 4177−4185.

MA020755L